CHEST IMAGING
Iran J Radiol. 2023 April; 20(2):e131348. https://doi.org/10.5812/iranjradiol-131348.
Published online 2023 April 24. **Research Article**

Application of Spectral Computed Tomography (CT) Combined with Conventional CT Features in Differentiating Malignant Pulmonary Mass-Like Lesions

Luyun Chen [1] and Yuanyi Huang [1,*]

[1]Department of Radiology, Jingzhou Hospital Affiliated to Yangtze University, Jingzhou, China

[*]*Corresponding author*: Jingzhou Hospital Affiliated to Yangtze University, Jingzhou, China. Email: 980527053@qq.com

Received 2022 September 03; **Revised** 2023 March 14; **Accepted** 2023 March 24.

Abstract

Background: Pulmonary mass-like lesions are one of the common manifestations of respiratory disorders. Differential diagnosis of these lesions is a major challenge in imaging studies.
Objectives: This study aimed to explore the efficacy of spectral computed tomography (CT) features combined with conventional CT features in the differential diagnosis of pulmonary mass-like lesions.
Patients and Methods: This case-control study was performed on a malignant group consisting of patients and a benign group consisting of controls. The imaging characteristics and spectral CT parameters were evaluated in 77 patients who met the inclusion criteria. A multivariate logistic regression analysis was performed to determine independent predictors of malignant pulmonary lump-like lesions. Three models were established, including a radiomic feature model, a spectral CT model, and a combined model. A receiver operating characteristic (ROC) curve was also plotted to evaluate the diagnostic efficiency of the models.
Results: Some CT features were significantly different between the malignant and benign groups, including the long-axis diameter (44.86 ± 18.42 in the malignant group vs. 55.59 ± 22.57 in the benign group; P = 0.07), mediastinal lymphadenopathy (25.00% in the benign group vs. 62.26% in the malignant group; P = 0.02), and mediastinal lymph node confluence (4.17% in the benign group vs. 41.51% in the malignant group; P = 0.01). The CT values at 40 keV (157.25 ± 79.23 vs. 148.46 ± 25.36, P = 0.047) and K40 - 70 keV (2.76 ± 2.05 vs. 2.52 ± 0.60, P = 0.04) were significantly higher in the benign group compared to the malignant group in the arterial phase (AP). Besides, the iodine concentration (IC) (14.73 ± 10.65 vs. 13.44 ± 3.24, P = 0.039; 17.52 ± 5.29 vs. 13.87 ± 5.81, P = 0.035), normalized iodine concentration (NIC) (0.15 ± 0.06 vs. 0.11 ± 0.05, P = 0.015; 0.41 ± 0.11 vs. 0.35 ± 0.10, P = 0.017), and Zeff value (8.46 ± 0.63 vs. 8.43 ± 0.28, P = 0.034; 8.60 ± 0.29 vs. 8.39 ± 0.33, P = 0.035) were significantly higher in the benign group compared to the malignant group, both in the AP and venous phase (VP). The logistic regression model, integrating CT features and spectral CT parameters, showed the highest diagnostic efficacy (area under the curve [AUC], 0.956; sensitivity, 87.5%; specificity, 90.6%).
Conclusion: The quantitative spectral CT parameters, combined with conventional CT features, could help distinguish benign and malignant pulmonary mass-like lesions, providing an essential basis for developing treatment plans.

Keywords: Benign Pulmonary Lesions, Malignant Pulmonary Lesions, Computed Tomography, Spectral CT

1. Background

Pulmonary mass-like lesions are one of the common manifestations of respiratory diseases, requiring a differential diagnosis. It is critical for clinicians to confirm the diagnosis of pulmonary mass-like lesions for early and accurate therapeutic planning. However, differential diagnosis is a major difficulty in imaging studies. In the big data era, precision medicine has been the focus of clinical studies. As a new examination technology, spectral computed tomography (CT) not only provides valuable information on the morphological characteristics of lesions and their enhancement patterns to facilitate a qualitative or quantitative assessment for tumor detection, characterization, staging, and efficacy analysis, but also yields single-energy virtual images and several quantitative parameters, such as iodine concentration (IC), slope of the energy spectrum curve, and effective atomic number (Zeff), using a substance-separation technology for a more accurate analysis of the lesion components (1). The results of previous studies suggest that spectral CT scan can play a crucial role in pathological staging (2-4), while there are few studies on the application of spectral CT for the detection of mass-like lesions of the lungs.

2. Objectives

The present study aimed to investigate the differential diagnostic value of spectral CT parameters combined with enhanced CT imaging features in detecting mass-like lesions of the lungs.

3. Patients and Methods

3.1. Patients

In this case-control study, the malignant group consisted of malignant cases, and the benign group consisted of the controls. There were 358 suspected cases, collected from November 2021 to May 2022 in Jingzhou Hospital, affiliated to Yangtze University, Hubei, China. Pathological examinations were performed on 75 patients who met the inclusion criteria, including 22 benign and 53 malignant cases. Two patients without pathological examination recovered using an anti-inflammatory treatment, and there was no recurrence (clinically confirmed inflammatory lesions) during the six-month follow-up. The benign group mainly included cases of pneumonia, inflammatory pseudotumor, tuberculosis, granulomatous inflammation, and cryptogenic organizing pneumonia. On the other hand, the malignant group included cases of adenocarcinoma, squamous cell carcinoma, and neuroendocrine tumors.

The inclusion criteria were as follows: (1) detection of mass-like lung lesions without any drug or surgical treatments before examination; (2) no history of adverse reactions to iodine contrast; (3) no history of hyperthyroidism, severe liver disorder, or renal insufficiency; (4) cases confirmed by surgery or aspiration pathology, as well as inflammatory cases observed in clinical follow-ups for lesion size reduction or disappearance; and (5) ability to cooperate with spectral CT imaging in the gemstone spectral imaging (GSI) mode. The image quality met the requirements for diagnosis and reconstruction.

This study was approved by the Medical Ethics Committee of Jingzhou Hospital, affiliated to Yangtze University (protocol number: 2022-073-01).

3.2. Image Acquisition

All the patients were examined in the GSI mode of the GE Revolution 256 CT scanner. The parameters were set as follows: Rotation time, 0.6 seconds; tube current, 600 mA; tube voltage, 80 kV/140 kV (instantaneous switching); and reconstruction layer thickness, 0.9 mm/0.9 mm. The entire lung field was swept from the first rib to the level of the diaphragm. Through the median elbow vein, 300 mg/mL of Ioversol was injected using a high-pressure syringe at a dose of 1.5 mL/kg (flow rate, 3 mL/sec), followed by the injection of 30 mL of saline at the same flow rate; the scan delay time after contrast injection was 30 and 60 seconds, respectively.

3.3. Image Feature Analysis and Quantitative Measurement of DECT Data

Two senior physicians jointly reviewed the films and measured the quantitative parameters using the GSI Viewer software, without any knowledge of the clinical and pathological findings. They analyzed the enhanced CT features of each lesion, including the tumor location, maximum cross-sectional lesion diameter, presence of uniform enhancement, internal structures (e.g., air bronchogram sign and cavity), and the surrounding structures. Regions of interest (ROI) was drawn to encompass more than two-thirds of the solid component of the lesion, avoiding vessels, calcification, or necrotic changes. The ROI data were measured at three adjacent image levels, and then, the mean value was calculated. Besides, the Zeff value was measured on the 40- and 70-keV monochromatic images in the arterial phase (AP) and venous phase (VP). The slope of the spectral curve between 40 keV and 70 keV was also calculated ([Hu40keV-Hu70keV]/30). The IC was measured according to the iodine map at the arterial and venous ROIs, and the normalized iodine concentration (NIC) was calculated based on the pulmonary artery IC at the same level of the lesion as the standard.

3.4. Statistical Analysis

All collected data were analyzed in SPSS Version 25.0 (IBM SPSS Statistics for Windows, released in 2017, IBM Corp., Armonk, NY, USA). Normally distributed quantitative data are expressed as mean ± standard deviation (SD), while non-normally distributed data are expressed as median ± interquartile range (IQR). Categorical data in both groups were analyzed using chi-square test, and continuous variables were compared using student's *t*-test (data with a normal distribution) and Mann-Whitney U test (data without a normal distribution), respectively. Additionally, a multifactorial logistic regression analysis was performed to determine the efficacy of CT features alone and CT features combined with spectral CT indices as independent predictors and to identify the optimal regression model for distinguishing benign and malignant lesions based on the area under the curve (AUC). Differences were considered statistically significant at a two-tailed P-value below 0.05.

4. Results

4.1. Patients

The clinical data of the patients are summarized in Table 1.

Table 1. Clinical Characteristics of the Patients in the Malignant and Benign Groups [a, b]

Variables	Benign group (n = 24)	Malignant group (n = 53)	P-value
Age	60.13 ± 11.64 [c]	67.40 ± 8.30 [c]	0.04
Sex			
Male	20	37	0.21
Female	4	16	
Smoking history	15	23	0.12
Clinical symptoms			
Fever	7	1	0.001
Cough	16	36	0.913
Coughing sputum	10	28	0.364
Chest pain	4	14	0.349
Laboratory tests			
Elevated leukocyte count	4	6	0.518
Elevated C-reactive protein level ($n_1 = 23$, $n_2 = 31$)	7	11	0.192

[a] n_1, Number of cases undergoing C-reactive protein tests in the benign group.
[b] n_2, Number of cases undergoing C-reactive protein tests in the malignant group.
[c] Mean ± standard deviation.

4.2. Conventional CT Characteristics of the Patients in the Benign and Malignant Groups

According to the univariate analysis, some CT features were significantly different between the malignant and benign groups, including the long-axis diameter (44.86 ± 18.42 in the malignant group vs. 55.59 ± 22.57 in the benign group, P = 0.07), thickened adjacent vessel (58.33% in the benign group vs. 5.66% in the malignant group, P = 0.001), pleural retraction (29.17% in the benign group vs. 69.81% in the malignant group, P = 0.001), mediastinal lymphadenopathy (25.00% in the benign group vs. 62.26% in the malignant group, P = 0.02), mediastinal lymph node confluence (4.17% in the benign group vs. 41.51% in the malignant group, P = 0.01), and lesion diameter-mediastinum relationship (parallel relationship: 58.33% in the benign group vs. 20.75.% in the malignant group, P = 0.001) (Table 2).

4.3. Comparison of Gemstone Spectral Imaging Parameters

Comparison of quantitative spectral CT parameters between the two groups is shown in Table 3.

Some spectral CT parameters in AP were significantly higher in the benign group compared to the malignant group, including CT values in 40 keV (157.25 ± 79.23 vs. 148.46 ± 25.36, P = 0.047) and K40-70 keV (2.76 ± 2.05 vs. 2.52 ± 0.60, P = 0.04). Besides, the IC (14.73 ± 10.65 vs. 13.44 ± 3.24, P = 0.039; 17.52 ± 5.29 vs. 13.87 ± 5.81, P = 0.035), NIC (0.15 ± 0.06 vs. 0.11 ± 0.05, P = 0.015; 0.41 ± 0.11 vs. 0.35 ± 0.10, P = 0.017), and Zeff (8.46 ± 0.63 vs. 8.43 ± 0.28, P = 0.034; 8.60 ± 0.29 vs. 8.39 ± 0.33, P = 0.035) in the benign group were significantly higher than those of the malignant group, both in the AP and VP. Figures 1 and 2 show the post-processed images of typical benign and malignant cases, respectively.

4.4. Multivariate Logistic Regression Analysis

According to the multivariate logistic regression analysis, the model of morphological characteristics included the lesion diameter, adjacent vessel thickening, and pleural depression sign, with a Cox-Snell R^2 value of 0.485. The model of quantitative spectral CT parameters included the effective atomic number in the arterial phase, with a Cox-Snell R^2 value of 0.139. Additionally, the combined model included IC in the arterial phase, effective atomic number in the arteriovenous phase, adjacent vessel thickening, pleural depression sign, lesion-mediastinum relationship, and mediastinal lymph node fusion, with a Cox-Snell R^2 value of 0.536.

The efficacy of each model in the differential diagnosis of benign and malignant pulmonary mass-like lesions was examined by the ROC curve analysis, the results of which are shown in Table 4. Except for the image feature model with the highest sensitivity, the AUC and specificity of the combined model were higher than the other two groups, and its diagnostic performance was relatively good (Table 4 and Figure 3).

Table 2. Association of CT Characteristics with Benign and Malignant Pulmonary Lesions

CT characteristics	Benign group (n = 24)	Malignant group (n = 53)	OR (95% CI)	t/χ^2	P-value
Location					
Upper lobe	11	35	0.435 (0.163 - 1.164)	2.804	0.094
Middle and lower lobes	13	18			
Long-axis diameter (mm)	44.86 ± 18.42 [a]	55.59 ± 22.57 [b]		-2.683	0.007
Internal					
Air space	7	13	1.267 (0.430 - 3.731)	0.185	0.667
Air bronchogram	1	2	1.109 (0.096 - 12.853)	0.007	0.934
Enhancement heterogeneity					
Homogeneous	4	4		- 0.374	0.708
Slightly or moderately heterogeneous	6	13			
Marked heterogeneity	14	26			
Surrounding structure					
Thickened adjacent vessel	14	3	23.333 (5.641 - 96.514)	26.641	0.001
Peripheral emphysema	4	20	0.330 (0.099 - 1.105)	3.418	0.064
Peripheral fibrosis	24	50	1.060 (0.992 - 1.132)	1.414	0.234
Lesion margin-pleura relationship					
Wide based	11	16	1.957 (0.724 - 5.289)	1.776	0.183
Narrow based	13	37			
Pleural retraction	7	37	0.178 (0.062 - 0.513)	11.143	0.001
Lesion diameter-mediastinum relationship					
Parallel	14	11	5.345 (1.874 - 15.252)	10.639	0.001
Vertical	10	42			
Mediastinal lymphadenopathy	6	33	0.202 (0.069 - 0.594)	9.177	0.002
Mediastinal lymph node fusion	1	22	0.061 (0.008-0.488)	10.997	0.001
Pleural effusion	2	10	0.391 (0.079 - 1.942)	1.394	0.238

Abbreviations: OR, odds ratio; CI, confidence interval.
[a] Median ± interquartile range.
[b] Mean ± standard deviation.

5. Discussion

As the method of choice for lung cancer screening, CT examination of the chest indicates the morphological features of lesions and enhancement patterns, which are of great importance in clinical practice. The results of previous studies have shown that virtual monoenergetic or monochromatic imaging (VMI) using spectral CT substance-separation techniques can replace conventional CT imaging to some extent, while reducing the radiation dose (5). With the application of spectral CT in life sciences, post-processing techniques can be employed in addition to morphological parameters to determine quantitative parameters and other clinical diagnostic indices, which provide further information about the lesions.

The present study showed that adjacent vessel thickening was more frequently combined with other signs in the benign group compared to the malignant group, based on the univariate analysis of imaging features. The benign group in the current study mainly included inflammatory lesions. Inflammatory mediators, such as inflammatory cytokines, chemokines, and vasoactive amines released from inflammatory tissues, may increase vascular permeability and contribute to vasodilatation. Although infiltrating cells are different in acute and chronic inflammations, the persistence of inflammatory factors is common in both (6). The accelerated tissue growth and metabolism of tumor lesions, continuous cell proliferation, and increased oxygen demand and blood supply requirement can lead to the thickening of blood supply arteries. With

Table 3. Comparison of Quantitative Spectral Computed Tomography (CT) Parameters Between the Groups [a]

Variables	CT values at 40 keV	CT values at 70 keV	IC	NIC	K40-70 keV	Zeff
Arterial phase						
Benign group (n = 24)	157.25 ± 79.23 [b]	79.63 ± 15.17 [c]	14.73±10.65 [b]	0.14 ± 0.10 [b]	2.76 ± 2.05 [b]	8.46 ± 0.63 [b]
Malignant group (n = 53)	148.46 ± 25.36 [c]	72.80 ± 10.63 [c]	13.44 ± 3.24 [c]	0.12 ± 0.05 [b]	2.52 ± 0.60 [c]	8.43 ± 0.28 [c]
T	1.991	1.997	2.068	2.442	2.051	2.117
P-value	0.047	0.054	0.039	0.015	0.04	0.034
Venous phase						
Benign group (n = 24)	176.45 ± 40.50 [c]	81.93 ± 15.62 [c]	17.52 ± 5.29 [c]	0.41 ± 0.11 [c]	3.15 ± 1.26 [c]	8.60 ± 0.29 [c]
Malignant group (n = 53)	158.42 ± 36.72 [c]	78.50 ± 16.45 [c]	13.87 ± 5.81 [c]	0.35 ± 0.10 [c]	2.76 ± 1.05 [b]	8.39 ± 0.33 [c]
T	1.784	1.626	2.149	2.433	1.199	2.141
P-value	0.078	0.108	0.035	0.017	0.231	0.035

Abbreviations: IC, iodine concentration; NIC, normalized iodine concentration.
[a] Zeff: Effective atomic number.
[b] Median ± interquartile range.
[c] Mean ± standard deviation.

Table 4. Diagnostic Performance of the Three Models Based on the Receiver Operating Characteristic (ROC) Curve Analysis for Distinguishing Benign and Malignant Lung Mass-Like Lesions

Variables	AUC	95% CI	P-value	Sensitivity	Specificity	PPV	NPV
Image feature model	0.921	0.849 - 0.994	0.001	0.917	0.868	0.939	0.826
Energy spectral CT parameter model	0.651	0.510 - 0.793	0.034	0.458	0.868	0.885	0.420
Combined model	0.956	0.912 - 1.000	0.001	0.875	0.906	0.954	0.766

Abbreviations: PPV, positive predictive value; NPV, negative predictive value; AUC, area under the curve; CI, confidence interval.

the invasion of tumor cells into the vessel wall, leading to luminal narrowing or even occlusion, the blood supply is less abundant than that of inflammatory lesions.

In the current study, most peripheral lung cancers were associated with adjacent pleural retraction due to fibrous tissue contraction within the lesion, although several inflammatory groups could also cause pleural reactions due to inflammatory exudation, resulting in localized pleural thickening and adhesion. Pleural retraction was more common in the malignant group; therefore, it might be used as a useful marker for distinguishing benign and malignant mass-like lesions of the lungs. Although some imaging manifestations of the two groups overlapped, some characteristic CT manifestations that could help with the differential diagnosis included the larger diameter of the lesion, proximity of pleural retraction, perpendicularity of the lesion to the mediastinum, and combination of mediastinal lymph node enlargement with mediastinal lymph node confluence, which often suggested lung cancer. The AUC in the multivariate logistic regression analysis was 0.921, which indicated the clinical value of enhanced CT imaging parameters in the differential diagnosis of benign and malignant mass-like lesions of the lungs.

The most significant advantage of spectral CT over conventional CT is the possibility of obtaining single-energy virtual images and substance-separation images through post-processing (7). By using iodine-water as the base material pair, the iodine maps are plotted using the substance-separation technique to determine the tissue IC, which can provide a more objective and quantitative analysis of the lesion components. The results of this study showed that CT values at 40 keV and K40-70 keV in the AP phase and IC, NIC, and Zeff values in the arteriovenous phase were higher in the benign group compared to the malignant group ($P < 0.05$); this finding is consistent with the results of a study by Hou et al. (8). Iodine, as the main component of the contrast agent, can reflect the tissue hemodynamic state; therefore, it is a more sensitive and realistic index for reflecting the degree of tissue enhancement compared to CT values. Besides, NIC can reduce individual differences caused by differences in the contrast flow rate and individual circulation and is more accurate than IC (9).

The blood supply to inflammatory lesions differs from cancerous lesions, as blood is supplied by both pulmonary and bronchial arteries. Second, inflammatory mediators

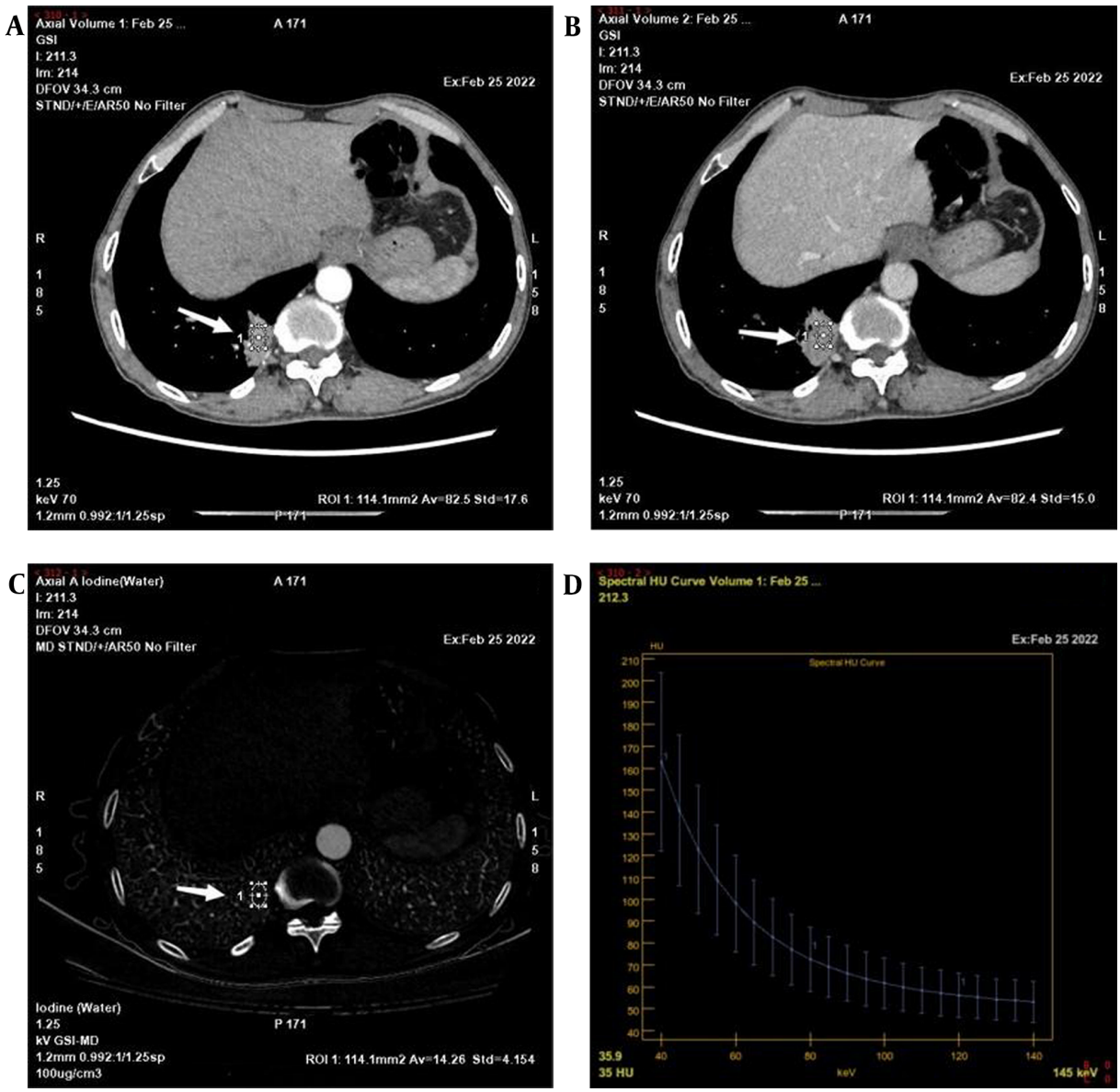

Figure 1. A-D, A 58-year-old man with granulomatous inflammation of the right lower lung, indicated by a white arrows. A-B, A 70-keV single-energy image in the arteriovenous phase; a mass-like high-density shadow can be seen in the right lower lobe of the lung next to the spine with adjacent bronchial occlusion. C, Iodine map in the arteriovenous phase; the iodine concentration (IC) of the lesion in the arteriovenous phase is 14.26 $\mu g/cm^3$. D, Arterial phase energy spectral graph.

released from inflammatory lesions can cause peripheral vasodilation, increase vascular permeability and edema in the adjacent tissues, and significantly increase perfusion in the lesion. Third, bronchial dilation near inflammatory lesions in the chronic phase is more pronounced than lung cancer. Overall, these factors can cause the inflamed tissue to have a better blood supply than cancerous lesions (10). Consistent with previous reports in the literature, suggesting that the slope of the energy spectrum curve in the AP and VP is significantly higher in inflammatory lung lesions compared to lung cancers (11), the energy spectral curve describes the attenuation of material under different energy X-ray irradiations and is closely related to the material density. The slope of the energy spectral curve in the AP and VP indicates that the blood supply of benign lung lesions is different from that of the malignant group, based on the quantitative analysis (12). The results of this study suggest that spectral CT parameters can be used as reliable indica-

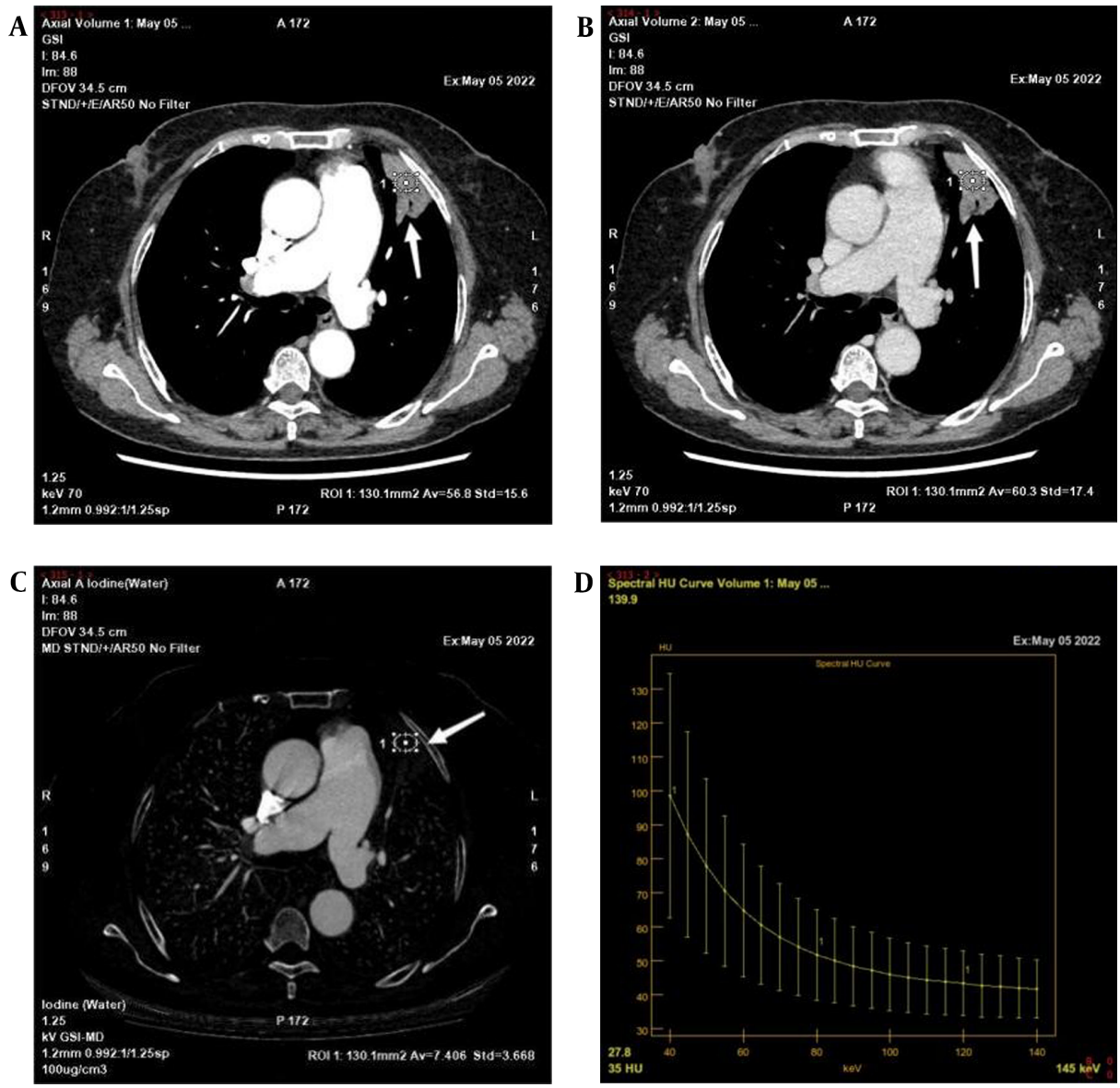

Figure 2. A-D, A 66-year-old man with adenocarcinoma of the left upper lung, indicated by a white arrows. A-B, A 70-keV single-energy image in the arteriovenous phase; a mass shadow of the left upper lobe of the lung can be seen with a cavity within it. C, An iodine base image in the arterial phase; the iodine concentration (IC) of the lesion in the arterial phase is 7.406 μg/cm^3. D, Arterial phase energy spectral graph.

tors for diagnosis of inflammatory diseases and cancers.

To further validate the diagnostic value of quantitative spectral CT parameters in the diagnosis of benign and malignant pulmonary mass-like lesions, a combined model was established by using these parameters along with morphological CT features. The results showed that the AUC of the combined diagnostic model was higher than that of the CT features model. The diagnostic performance of the combined model was superior, which might help improve the diagnostic accuracy.

This study had some limitations. First, the sample size was small, especially the number of benign cases; therefore, further data collection is needed in the future. Second, mass-like lesions of different sizes were not subdivided in this study, and different tumor stages were not analyzed in further detail. Overall, the sample size needs to be increased for a more comprehensive analysis in follow-up studies.

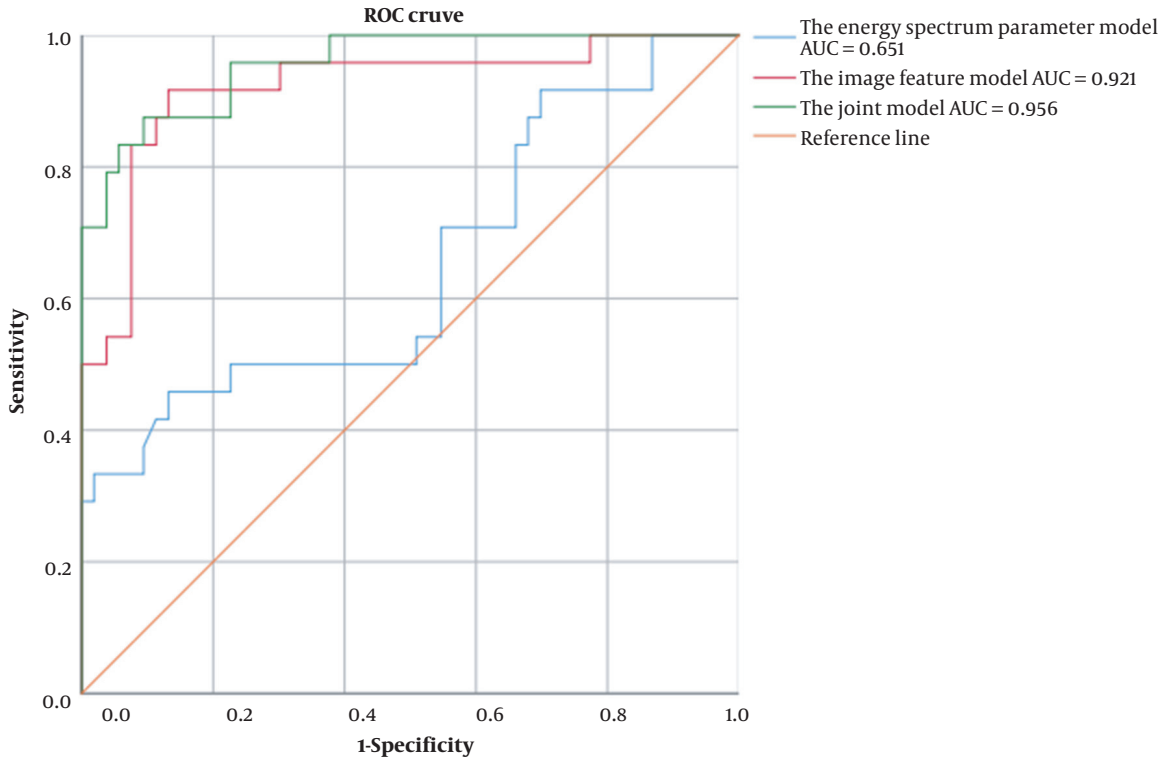

Figure 3. The receiver operating characteristic (ROC) curves of the logistic regression models (AUC: Area under the curve)

In conclusion, compared to the CT features alone, the combination of CT features with quantitative spectral CT parameters showed a superior diagnostic performance. This combination was a powerful predictive index for the differential diagnosis of pulmonary mass-like lesions, which can non-invasively provide additional information for the preoperative therapeutic evaluation of patients with lung diseases and help clinicians select the best treatment plan.

Footnotes

Authors' Contribution: C. L. Y. conceived and designed the assessments and drafted the manuscript. H. Y. Y. participated in designing the assessments, performed the statistical analysis, and helped draft the manuscript. H. Y. Y. re-analyzed the clinical and statistical data and revised the manuscript. All authors read and approved the final manuscript.

Conflict of Interests: The authors have no conflicts of interest to declare that are relevant to the content of this article.

Data Reproducibility: The dataset presented in this study is available on request from the corresponding author during submission or after publication.

Ethical Approval: This study was approved by the Medical Ethics Committee of Jingzhou Hospital, affiliated to Yangtze University (protocol number: 2022-073-01).

Funding/Support: This research did not receive any specific grant from any funding agencies in the public, commercial, or not-for-profit sectors.

Informed Consent: Informed consent was obtained from the participants of this study.

References

1. Rajiah P. Dual-energy computed tomography in thoracic imaging-current practices and utility: Survey of the society of thoracic radiology. *J Thorac Imaging*. 2020;**35**(2):W43–50. [PubMed ID: 31584479]. https://doi.org/10.1097/RTI.0000000000000450.
2. Dou P, Liu Z, Xie L, Meng C, Wang C, Cui Y, et al. The predictive value of energy spectral CT parameters for assessing Ki-67 expression of lung cancer. *Transl Cancer Res*. 2020;**9**(7):4267–78. [PubMed ID: 35117793]. [PubMed Central ID: PMC8798171]. https://doi.org/10.21037/tcr-19-2769a.

3. Li Q, Li X, Li XY, He XQ, Chu ZG, Luo TY. Histological subtypes of solid-dominant invasive lung adenocarcinoma: Differentiation using dual-energy spectral CT. *Clin Radiol*. 2021;**76**(1):77 e1–7. [PubMed ID: 33121736]. https://doi.org/10.1016/j.crad.2020.08.034.
4. Zhu B, Zheng S, Jiang T, Hu B. Evaluation of dual-energy and perfusion CT parameters for diagnosing solitary pulmonary nodules. *Thorac Cancer*. 2021;**12**(20):2691–7. [PubMed ID: 34409741]. [PubMed Central ID: PMC8520802]. https://doi.org/10.1111/1759-7714.14105.
5. Sauter AP, Muenzel D, Dangelmaier J, Braren R, Pfeiffer F, Rummeny EJ, et al. Dual-layer spectral computed tomography: Virtual non-contrast in comparison to true non-contrast images. *Eur J Radiol*. 2018;**104**:108–14. [PubMed ID: 29857855]. https://doi.org/10.1016/j.ejrad.2018.05.007.
6. Zhao H, Wu L, Yan G, Chen Y, Zhou M, Wu Y, et al. Inflammation and tumor progression: Signaling pathways and targeted intervention. *Signal Transduct Target Ther*. 2021;**6**(1):263. [PubMed ID: 34248142]. [PubMed Central ID: PMC8273155]. https://doi.org/10.1038/s41392-021-00658-5.
7. Hamid S, Nasir MU, So A, Andrews G, Nicolaou S, Qamar SR. Clinical applications of dual-energy CT. *Korean J Radiol*. 2021;**22**(6):970–82. [PubMed ID: 33856133]. [PubMed Central ID: PMC8154785]. https://doi.org/10.3348/kjr.2020.0996.
8. Hou WS, Wu HW, Yin Y, Cheng JJ, Zhang Q, Xu JR. Differentiation of lung cancers from inflammatory masses with dual-energy spectral CT imaging. *Acad Radiol*. 2015;**22**(3):337–44. [PubMed ID: 25491737]. https://doi.org/10.1016/j.acra.2014.10.004.
9. Li Q, Li X, Li XY, Huo JW, Lv FJ, Luo TY. Spectral CT in lung cancer: Usefulness of iodine concentration for evaluation of tumor angiogenesis and prognosis. *AJR Am J Roentgenol*. 2020;**215**(3):595–602. [PubMed ID: 32569515]. https://doi.org/10.2214/AJR.19.22688.
10. Liang G, Yu W, Liu SQ, Xie MG, Liu M. The value of radiomics based on dual-energy CT for differentiating benign from malignant solitary pulmonary nodules. *BMC Med Imaging*. 2022;**22**(1):95. [PubMed ID: 35597900]. [PubMed Central ID: PMC9123722]. https://doi.org/10.1186/s12880-022-00824-3.
11. Zhu LH, Wang FN, Wang YW, Cheng QH, Zhou JJ. Differentiation between solitary pulmonary inflammatory lesions and solitary cancer using gemstone spectral imaging. *J Comput Assist Tomogr*. 2022;**46**(2):300–7. [PubMed ID: 35081600]. https://doi.org/10.1097/RCT.0000000000001268.
12. Zhang Y, Cheng J, Hua X, Yu M, Xu C, Zhang F, et al. Can spectral CT imaging improve the differentiation between malignant and benign solitary pulmonary nodules? *PLoS One*. 2016;**11**(2). e0147537. [PubMed ID: 26840459]. [PubMed Central ID: PMC4739615]. https://doi.org/10.1371/journal.pone.0147537.